Kinesin Binding Protein (KBP) buffers the activity of Kif18A and Kif15 in mitosis to ensure accurate chromosome segregation

Heidi L. H. Malaby[1], Megan Dumas[2], Ryoma Ohi[2,3,4*], and Jason Stumpff[1*]

[1] Department of Molecular Physiology and Biophysics, University of Vermont, Burlington, VT 05405, United States
[2] Department of Cell and Developmental Biology, Vanderbilt University Medical School, Nashville, TN 37232, United States
[3] The Life Sciences Institute, University of Michigan Medical School, Ann Arbor, MI 48109, United States
[4] Department of Cell and Developmental Biology, University of Michigan Medical School, Ann Arbor, MI 48109, United States
[*] Corresponding authors: jstumpff@uvm.edu and oryoma@umich.edu

RUNNING TITLE

KBP buffers Kif18A and Kif15 activity in mitosis

SUMMARY

Kinesin Binding Protein (KBP) is identified as mitotic regulator of the kinesins Kif18A and Kif15, buffering the activity of these kinesins to control chromosome alignment and spindle integrity in metaphase and protecting against lagging chromosomes in anaphase.

ABSTRACT

Mitotic kinesins must be regulated in mitosis to ensure a precise balance of spindle forces and accurate segregation of chromosomes into daughter cells. Here we characterize Kinesin Binding Protein (KBP) function in metaphase and show it regulates the kinesins Kif18A and Kif15. KBP expression impacts chromosome alignment and spindle length, both phenotypes observed in cells deficient of Kif18A and Kif15, and affects spindle integrity and kinetochore oscillations. We show through gliding filament and microtubule co-pelleting assays that KBP directly inhibits Kif18A and Kif15 motor activity by preventing microtubule-binding. The localizations of Kif18A and Kif15 are affected by overexpression of KBP, which we show is dominantly cytosolic in cells. Cells deficient in KBP regulation have multiple lagging chromosomes in anaphase, an effect that is recapitulated by Kif15 and Kif18A overexpression. We propose a model were KBP acts as a protein buffer in mitosis, protecting cells from excess activity of Kif18A and Kif15 to ensure accurate segregation of chromosomes.

INTRODUCTION

Kinesin motor proteins are the workhorses of mitosis, providing forces required for chromosome alignment and equal separation through a finely-tuned balancing act (Cross and McAinsh, 2014). Each of the known 16 human mitotic kinesins must provide their contribution not only at a specific location within the spindle, but also at very specific times throughout the mitotic cycle (Rath and Kozielski, 2012). While many of the mitotic kinesins have unique intrinsic structural differences that provide this specificity, there are also a

number of extrinsic regulators of the kinesin family that provide additional checks and balances of their function (Yount et al., 2015). These include proteins that localize subsets of kinesins to specific areas of the cell, like kinesin-4 (Kif4A) and PRC1 driven central spindle scaffolding to recruit kinesin-6 (MKLP1 and MKLP2), kinesin-7 (CENP-E) and kinesin-3 (Kif14) to midzone microtubules in anaphase (Kurasawa, 2004; Zhu and Jiang, 2005). EB1 recruits kinesin-13 (MCAK), kinesin-8 (Kif18B), and kinesin-5 (Eg5) to microtubule plus-ends (Honnappa et al., 2009; Jiang et al., 2012; Stout et al., 2011). Importin α/β recruits kinesin-13 (MCAK) kinesin-6 (MKLP1), kinesin-8 (Kif18A), kinesin-10 (KID), and kinesin-14 (HSET/XCTK2) to the nucleus prior to mitotic onset and Ran gradient regulation during mitosis (Du et al., 2010; Ems-McClung et al., 2004; Nachury et al., 2001; Tahara et al., 2008; Wordeman et al., 1999). CHICA specifically recruits kinesin-10 (KID) to the spindle (Santamaria et al., 2008), and TPX2 stabilizes kinetochore microtubules promoting the recruitment of kinesin-5 (Eg5) and kinesin-12 (Kif15) (Ma et al., 2011; Mann et al., 2017; Sturgill et al., 2014; Tanenbaum et al., 2009). These regulatory proteins are necessary for localizing their active kinesin substrates to their required setting during mitosis.

Kinesin activity can also be regulated via direct binding to inhibitory proteins. Kinesin-binding protein (KBP) was first identified as a disease-causing gene (dubbed *KIAA1279*) through genetic sequencing of patients with Goldberg-Shprintzen Syndrome, a disorder marked by microcephaly, mental retardation, and facial dysmorphism (Alves et al., 2010; Brooks et al., 2005; Drevillon et al., 2013). Due to it's clear neurological ties, KBP function has been studied in neurons and found to be a direct inhibitor of the kinesin-3 family member Kif1Bα, which is necessary for proper mitochondrial transport down the axon (Wozniak et al., 2005). More recently, an extensive biochemical study was conducted to determine KBP specific binding to a large panel of human kinesins (Kevenaar et al., 2016). In addition to kinesin-3 family members (Kif1A, Kif1B, Kif1C, and Kif14), KBP was also found to have strong affinity for kinesin-2 family members (Kif3A and Kif3B), a kinesin-8 (Kif18A) and a kinesin-12 (Kif15). Further, KBP was found to interact directly with these kinesin's motor domain with a 1:1 KBP:motor domain stoichiometry, and that this direct binding blocks the kinesins ability to interact with the microtubule (Kevenaar et al., 2016).

Kif18A and Kif15 both have established roles in mitosis. Kif18A localizes to the ends of kinetochore microtubules and confines chromosomes to the spindle midzone by dampening kinetochore microtubule dynamics, which drive chromosome oscillations (Du et al., 2010; Stumpff et al., 2008). Kif15 maintains spindle integrity by mediating kinetochore microtubule separation forces (Sturgill and Ohi, 2013; Tanenbaum et al., 2009). KBP was identified as a candidate interactor of Kif18A and Kif15 from an affinity-purification mass spectrometry screen of BAC HeLa cells (Maliga et al., 2013), and was implicated in regulating Kif15 during mitosis (Brouwers et al., 2017), but KBP's mechanistic role and general importance as a mitotic kinesin regulator is not understood.

Here, we have determined that KBP inhibits the functions of the kinesins Kif18A and Kif15 in spindle regulation and chromosome alignment during mitosis and show that this inhibition occurs by preventing the kinesin's binding to microtubules. We have found the KBP itself is largely cytosolic in mitotic cells, and altered expression of KBP affects the localization of both Kif18A and Kif15. Further, inhibition of both kinesins by KBP is required to ensure the proper segregation of chromosomes during anaphase. We show that an excess of either Kif18A or Kif15 in the cell can result in lagging chromosomes during anaphase. We propose that KBP is present in mitosis to buffer kinesin activity, ensuring that a high threshold of activity is not exceeded for either Kif15 or Kif18A.

RESULTS

KBP expression level affects chromosome alignment and spindle length in mitotic cells

We first determined if KBP is expressed in dividing cells, and if so, where it localizes. HeLa cell extracts were prepared after knockdown with either a scrambled control siRNA or a KBP specific siRNA. By Western, a specific band near the 75 kDa marker is detected, and this is significantly reduced upon KBP siRNA treatment (Figure 1A). This is in agreement with the predicted molecular weight of KBP (72 kDa) and previous findings (Drevillon et al., 2013; Kevenaar et al., 2016; Wozniak et al., 2005). Endogenous KBP immunofluorescence did not reveal any structurally specific staining in mitotic cells, nor did an N-terminally mCherry tagged KBP construct at nominal levels (Figure 1B). In cells expressing high quantities of mCherry KBP, KBP was still largely cytosolic with occasional punctate spots co-localizing with microtubules (Figure 1B, inset). Mitotic cells expressing mCherry KBP showed faint pole and spindle staining, but otherwise the protein was cytosolic (Figure 1C).

We next asked if alteration of KBP protein levels affects mitotic spindle function. Cells were transfected with KBP siRNAs or mCherry KBP, arrested in MG132 to prevent entry into anaphase, fixed, and stained to visualize chromosomes, centromeres, centrosomes, and microtubules (Figure 1C). We identified aberrations in chromosome alignment and spindle length in metaphase cells. Chromosome alignment was quantified by measuring centromere (ACA) immunofluorescence signal along the spindle axis to determine the width of the fluorescence distribution at 50% of its full intensity (FWHM), a metric we have used previously (Kim et al., 2014; Stumpff et al., 2012). KBP siRNA treatment resulted in a significant portion of the population displaying hyper-alignment, a bilinear arrangement of sister kinetochores at the metaphase plate (Figure 1D, middle, dotted line indicates hyper-alignment cutoff of 3.3 μm). Conversely, mCherry KBP overexpression resulted in significantly unaligned chromosomes. This unalignment effect scaled proportionally with mCherry intensity (Figure 1D, right). We also found that spindle lengths were affected by KBP expression. KBP siRNA treatment resulted in a population of slightly longer spindles (average 11.8 μm vs. 12.2 μm), an effect amplified with mCherry KBP overexpression (12.7 μm, Figure 1E, left). Interestingly, spindle length also scaled in proportion with mCherry intensity, but trended in the opposite direction (Figure 1E, right), indicating that KBP inhibits mitotic kinesin motors that contribute to chromosome alignment and provide forces that push spindle poles apart. Together, these results identify a role for KBP in regulating chromosome alignment and spindle length during mitosis.

Co-depletion of Kif18A and Kif15 recapitulates the spindle length and chromosome alignment defects seen in KBP overexpressing cells

KBP was previously identified as a potential interactor of Kif18A, Kif15, and Kif14 from affinity-purification mass spectrometry analysis of mitotic kinesins, (Maliga et al., 2013), and these three mitotic motors were also characterized as KBP substrates by co-IPs (Kevenaar et al., 2016). We wished to determine if depletion of these motors, alone or in combination, could explain KBP's effects on chromosome alignment and spindle length. While Kif18A's influence of chromosome alignment (Du et al., 2010; Stumpff et al., 2008)

and Kif15's affect on spindle length (Sturgill and Ohi, 2013; Tanenbaum et al., 2009) are well established, a role for Kif14 in metaphase has not been clearly elucidated. We transfected cells with Kif14 siRNAs and stained for the endogenous protein (Figure S1A). We found that Kif14 was cytosolic in metaphase cells (Figure S1C) and localized to the midbody during telophase (Figure S1A). Importantly, both signals decreased following Kif14 siRNA treatment. We did not detect any effects on chromosome alignment or spindle length upon Kif14 knockdown (Figure S1B). These results narrowed our metaphase KBP kinesin substrates to only Kif18A and Kif15.

We next transfected cells with either Kif18A, Kif15, or Kif18A and Kif15 siRNAs, then fixed and stained cells to visualize centromeres, centrosomes, and chromosomes (Figure 2A and 2B). Two coverslips were made for every condition, allowing for detection and quantification of each endogenous motor in the double knockdown condition (Figure 2D). Chromosome alignment and spindle length were then analyzed as in Figure 1. Kif18A knockdown resulted in unaligned chromosomes (large FWHM values), and this phenotype remained unchanged in combination with Kif15 knockdown (Figure 2C, left). Both Kif18A and Kif15 individual knockdowns affected spindle length, with the former increasing and the latter decreasing spindle lengths. Interestingly, cells with combined Kif18A and Kif15 knockdown displayed spindle lengths on par with control cells (Figure 2C, right). These results confirm that inhibition of Kif18A and Kif15 in combination could generate the effects observed upon KBP overexpression in Figure 1, with the exception of spindle lengths being slightly longer on average in the mCherry KBP population. This finding indicates the KBP may inhibit Kif18A and Kif15 to different degrees.

KBP inhibits Kif18A motor activity more potently than Kif15 motor activity *in vitro*

Because mCherry KBP overexpression produced spindle lengths on average longer than the control condition, which was not observed in the Kif18A and Kif15 double knockdown, we sought to determine the KBP binding potency for each of these motors *in vitro*. KBP and C-terminally truncated Kif18A (Kif18A-N480) and Kif15 (Kif15-N700) were purified from *Sf*9 cells or *E. coli* (Figure S2) and analyzed for activity by gliding filament assays (Figure 3A and 3C, Videos S1-S4). For quantification of microtubule gliding inhibition, the velocity of single microtubules was divided by the average velocity of all motor-only control microtubules per experimental day, and subtracted from one hundred to determine the percent of inhibition. Our results confirm the previous finding that KBP inhibits the activity of both Kif15 and Kif18A (Kevenaar et al., 2016), and show that this inhibition occurs in a dose dependent manner (Figure 3B and 3D), with Kif18A showing enhanced sensitivity to KBP levels.

We asked whether this inhibition was the result of microtubule binding interference as has been reported for Kif1A (Kevenaar et al., 2016). For this assay, we pre-incubated motors with KBP to allow complex formation, and then mixed proteins with microtubules in the presence of AMPPNP. Under these conditions, we expected to capture the majority of kinesin motors in a microtubule-bound state in the absence of KBP. The motor constructs we used lack secondary microtubule-binding sites outside of the motor domain (Kif18A-N480 (Stumpff et al., 2011) and Kif15-N420 (Reinemann et al., 2017), ensuring that any effects of KBP on motor-microtubule interactions were likely to be mediated through the motor domain. In the absence of KBP, both Kif18A-N480 and Kif15-N420 co-pelleted with microtubules, with varying efficiencies. In the presence of microtubules and KBP, both motors shifted from the pellet to the supernatant. (> 90% for Kif18A, ~20% for Kif15). These

assays show that KBP is directly inhibiting Kif18A and Kif15 motor activity by blocking microtubule binding and that KBP is a more potent inhibitor of the Kif18A motor than the Kif15 motor.

KBP expression affects the localization of Kif18A and Kif15 on the mitotic spindle

We next determined if alterations in KBP expression affect the localization of Kif18A or Kif15 in mitotic cells. Cells were transfected with control or KBP siRNA or mCherry KBP, fixed, and stained for the endogenous motors Kif18A (Figure 4A) or Kif15 (Figure 4C). Kif18A localizes to and accumulates at kinetochore microtubule plus-ends, which can be measured by line scan analysis. Quantification of Kif18A localization was performed by combining 5-10 kinetochore microtubule line scans per cell analyzed. Fluorescence was normalized to the highest value for each wavelength, and individual line scans were aligned using the peak kinetochore (Hec1) signal. The average intensities for each channel are plotted in Figure 4B with standard deviations indicated. KBP knockdown did not significantly alter kinetochore microtubule end accumulation, however, mCherry KBP overexpression resulted in uniform spindle distribution of the endogenous motor.

Since Kif18A contains a second microtubule-binding site in its C-terminal tail (Mayr et al., 2011; Stumpff et al., 2011; Weaver et al., 2011), we hypothesized that this spindle localization phenotype in the presence of additional KBP might be due to tail microtubule binding. To test this, we transfected cells with either a GFP-tagged wild-type Kif18A full-length motor or a C-terminal truncation of Kif18A (18A Δ480) alongside mCherry KBP and quantified the ratio of spindle to cytoplasmic GFP intensity (Figure S3). In addition to confirming the spindle localization phenotype observed with the endogenous motor, the GFP-tagged full-length Kif18A expressed with mCherry KBP showed a significant increase in cytoplasmic motor (Figure S3B middle). This effect was independent of GFP-Kif18A expression level (Figure S1B right). Strikingly, GFP-tagged Kif18A Δ480 co-expressed with mCherry KBP abolished spindle localization, resulting in fully cytosolic motor (Figure S3A and S3B). This finding 1) confirms that Kif18A's C-terminal tail is necessary to maintain microtubule association when the motor is inhibited by KBP, 2) indicates that the Kif18A motor domain is unable to associate with microtubules when bound to KBP, similar to findings for the kinesin-3 motor Kif1A (Kevenaar et al., 2016), and 3) supports our earlier conclusion that KBP itself is cytosolic.

Endogenous Kif15 localizes to microtubules throughout the spindle, with a slightly higher concentration observed near the metaphase plate (Figure 4C). To quantify changes in Kif15 localization, we determined the width of Kif15's fluorescence distribution along the spindle axis at 50% of its full intensity, similar to the metric used to quantify chromosome alignment described in Figure 1. Kif15 localization was not significantly altered upon KBP knockdown but was distributed more evenly along the spindle in cells overexpressing mCherry KBP (Figure 4D). Overall, these findings confirm that KBP affects the localization of both Kif18A and Kif15 in mitosis.

KBP overexpression prevents Kif15-driven spindle stabilization

We next asked if KBP affects the specific functions of Kif15 and Kif18A in mitotic cells. Kif15 has a partially overlapping role in spindle bipolarity maintenance with Eg5 (Tanenbaum et al., 2009), but is necessary to maintain spindle integrity when Eg5 is inhibited (Sturgill et al., 2014; Tanenbaum et al., 2009). KBP does not bind Eg5 (Kevenaar

et al., 2016; Maliga et al., 2013). We transfected cells with either mCherry alone or mCherry KBP, and treated them with DMSO as a negative control or the Eg5 inhibitor STLC before fixation (Figure 5A). Metaphase cells were scored for bipolar or monopolar spindles in each population, and each transfection condition was normalized to the DMSO control. With Eg5 inhibited under the STLC condition, we observed over a two-fold increase in the number of monopolar spindles with mCherry KBP overexpression (Figure 5B). These results are consistent with KBP inhibition of Kif15's function in spindle stabilization in mitotic cells.

Alteration in KBP expression influences kinetochore oscillations

Kif18A accumulates at kinetochore microtubule plus-ends and suppresses microtubule dynamics, which contributes to the confinement of chromosomes near the metaphase plate (Du et al., 2010; Stumpff et al., 2008). Kif18A knockdown is known to increase the distance of kinetochores from the metaphase plate and the amplitude of kinetochore oscillations during metaphase, while Kif18A overexpression dampens oscillations (Stumpff et al., 2008). The effects can be assayed by measuring the deviation from the metaphase plate (DMP) and the deviation from average position (DAP) of kinetochores in live metaphase cells (Stumpff et al., 2008; Stumpff et al., 2012). To determine the effects of altered KBP expression on kinetochore oscillations, cells were transfected with either control or KBP siRNAs or plasmids encoding mCherry or mCherry KBP. All conditions included the additional transfection of GFP-tagged CENP-B to visualize individual kinetochores. Mitotic cells where then imaged using time-lapse microscopy (see Videos S5-S8), and analyzed by tracking kinetochore pairs. Figure 6A and 6B show representative kinetochore pair tracks and kymographs for all conditions. KBP knockdown showed a significant reduction in both the DMP and DAP compared to control knockdown cells (Figure 6C, black data). Despite the expression of mCherry alone being several fold higher than mCherry KBP in the cells analyzed, mCherry KBP overexpression significantly increased both the DMP and DAP measurements compared to mCherry alone (Figure 6C, red data). These results are consistent with KBP inhibiting Kif18A's function in controlling kinetochore oscillations.

KBP knockdown or Kif18A/Kif15 overexpression results in lagging chromosomes during anaphase

Lastly, we wished to determine the consequences of inhibiting KBP regulation on chromosome segregation. To assess this, we analyzed the frequency of lagging chromosomes in anaphase cells following KBP knockdown (Figure 7A). We detected a two-fold increase in anaphase cells with lagging chromosomes under KBP knockdown conditions (Figure 7B). Importantly, of the cells that contained lagging chromosomes, KBP knockdown cells were significantly more likely to have more than one or two lagging chromosomes in the cell (Figure 7C). These results show that KBP regulation is required for normal chromosome segregation.

To determine if this phenotype is reflective of excess Kif18A and Kif15 motor activity, we overexpressed either mCherry alone, mCherry-tagged Kif18A, GFP-tagged Kif15, or mCherry-tagged Kif18A and GFP-tagged Kif15 in combination. Cells were fixed, stained, and all anaphase cells expressing the above constructs were imaged (Figure 7D). We observed that overexpression of either mCherry-Kif18A or GFP-Kif15 could result in lagging

chromosomes, and that the likelihood of lagging chromosomes scaled proportionally with increasing fluorescence intensity (Figure 7E). In addition, we found that cells with the highest expression (top 25%) of mCherry-Kif18A or GFP-Kif15 alone or in combination were much more likely to have split poles in addition to multiple lagging chromosomes, particularly in the double motor overexpression condition (Figure 7F). To determine the fold-increase of motor in these overexpression conditions, we expressed either mCherry-Kif18A or GFP-Kif15 as above, but stained the cells with antibodies against the motor itself. In this way, we could monitor if a cell was expressing our additional kinesin motor, and then quantify the total amount of motor present in the cell. We found that our overexpression resulted in a ~1.5-fold increase in kinesin level in the cell (Figure 7G), a range that is on par with measured protein variations within a population (Sigal et al., 2006). Taken together, these results indicate that KBP inhibition of Kif18A and Kif15 is necessary to prevent lagging chromosomes during anaphase.

DISCUSSION

Here we have shown that KBP is an inhibitory regulator of Kif18A and Kif15 in mitosis and that this regulation is required for the proper segregation of chromosomes in anaphase. Altered KBP expression in metaphase cells disrupts chromosome alignment and shortens spindle length, and these effects can be explained by inhibition of Kif18A and Kif15 function. KBP expression inhibits Kif18A accumulation at kinetochore microtubule plus-ends, causing the localization of the motor across the spindle due to the Kif18A's C-terminal tail microtubule binding site. When this site is removed, both Kif18A and KBP are completely cytosolic. KBP inhibition of Kif15 also alters the motors localization to a more uniform distribution along the spindle, likely also due to its additional microtubule binding sites outside of the motor domain (Sturgill et al., 2014). KBP expression also influences the functions of both Kif18A in controlling chromosome oscillations and Kif15 in maintaining spindle integrity.

Recently, another study identified KBP as a regulator of Kif15 in mitosis (Brouwers et al., 2017), and that Kif15 helps to align chromosomes at the metaphase plate. This study concluded that KBP itself localizes to the spindle, a finding that contradicted single molecule TIRF evidence that KBP does not bind microtubules (Kevenaar et al., 2016). Our findings here, particularly the co-pelleting assays and localization of truncated Kif18A with mCherry KBP, support the earlier conclusion that KBP does not bind microtubules, but may interact with microtubules indirectly via kinesins that contain non-motor microtubule binding domains. In addition, interphase cells expressing mCherry-KBP display occasional puncta on microtubules (Figure 1B), which would be expected given the abundance of kinesin-2 and kinesin-3 motors present in mammalian interphase cells. Lastly, our Kif15 knockdown studies did not identify a role for Kif15 in chromosome alignment, a conclusion supported by other studies of Kif15 function in mitosis (Sturgill and Ohi, 2013; van Heesbeen et al., 2014).

Kif14 has also been identified as a potential substrate for KBP in mitosis (Maliga et al., 2013). Our study focused on KBP's influence on chromosome alignment and spindle length in metaphase and its consequences in anaphase. We did not observe any changes in these mitotic functions following Kif14 knockdown (Figure S2). However, Kif14 does have a well-established role in cytokinesis (Carleton et al., 2006; Gruneberg et al., 2006). The

possibility of KBP regulation of Kif14 during telophase and cytokinesis will be an enticing topic for future studies.

Our finding that KBP has a greater inhibitory effect on C-terminally truncated Kif18A over C-terminally truncated Kif15, which is also in agreement with previous immunoprecipitation assays between KBP and these motors (Kevenaar et al., 2016), suggests a higher KBP potency for the Kif18A motor domain over the Kif15 motor domain. This may explain the range of spindle lengths observed in Figure 1E, where KBP overexpression resulted in a cell population with longer spindle lengths on average even though strict knockdown of Kif18A and Kif15 in combination produces cells with normal spindle lengths (Figure 4C). A stronger preference for Kif18A compared to Kif15 could lead to the Kif18A dominant phenotype of longer than average spindles. When we look closer at the expression of KBP on an individual cell basis (Figure 1E, right), we see that increasing KBP expression trends to shorter spindles, consistent with decreasing Kif15 activity. Phosphorylation has also been shown to alter KBP binding for kinesin motors (Kevenaar et al., 2016), a possible transient or stable factor adding to the complexity of cellular studies, but warrants deeper future investigation. Why might KBP have evolved a higher potency for Kif18A? From Figure 7, we find that cells are less tolerant of Kif18A overexpression (more average lagging chromosomes and more split poles with increasing expression), providing a possible explanation that higher KBP potency is required to safeguard cells that are less tolerant of excess Kif18A than Kif15.

The regulation of both Kif18A and Kif15 by KBP is required to prevent lagging chromosomes in anaphase. Given the additional split pole phenotype observed from overexpression of Kif18A and Kif15, it is likely that these lagging chromosomes are caused by merotelic attachments, a common cause of segregation errors especially when the integrity of the spindle and control of chromosomal oscillations are compromised (Bakhoum and Compton, 2012). We have found that our kinesin overexpression assays only increase the population of Kif18A and Kif15 by about half (Figure 7G). Since the highest expressing phenotypes observed in these populations are split poles, an observation not seen upon KBP knockdown, it is likely that cells with lagging chromosomes in our kinesin overexpression assays are within the range of protein expression variability that naturally occurs in a cell population.

We propose a model where KBP is acting as a protein buffer in the mitotic system, acting through its varying affinity to specific kinesin substrates as a referee to maintain a steady level of Kif18A and Kif15 active motor on the spindle. Why would a mode of regulation evolve to inhibit specific kinesin function when there are clearly established modes of transcriptional, translational, and ubiquitin-mediated degradation regulation (Nath et al., 2015)? The process of equal segregation of chromosomes is brought about by very finely balanced forces within the spindle (Prosser and Pelletier, 2017), leaving very little wiggle room for variations in activity levels. Studies have found that protein variability can range within a cell population up to 30%, and that this variation is affected not just by the protein in question but can also vary significantly within the history of a single cell, which was shown by tracking protein expression through multiple generations (Sigal et al., 2006). We propose that KBP functions to ensure minor fluctuations in protein levels do not interfere with these precisely balanced forces, thus promoting robust and reproducible division of genetic material amongst protein expression variations within cells.

MATERIALS AND METHODS

Plasmids and siRNAs

mCherry-KBP and mCherry-Kif18A were constructed by Gateway Cloning Technology (Thermo Fisher Scientific). First, the KBP gene (HA-KBP plasmid received as a kind gift from Casper Hoogenraad) and Kif18A open reading frames were inserted into pCR8/GW/TOPO (Thermo Fisher Scientific). Correctly inserted clones were confirmed by sequencing. The KBP and Kif18A genes were then inserted by LR recominbation reaction (Thermo Fisher Scientific) into a pCMV *ccdB* destination vector containing an N-terminal mCherry gene in frame with R1/R2 recombination sites. Clones were screened by restriction digestion, and the full open reading frames were confirmed by sequencing. For protein expression, GST-KBP was constructed by isothermal assembly, where the full length human KBP cDNA (GE Healthcare, CloneId:4550085) was inserted into the pGEX6P1 vector (Amersham). Clones were screened by Sal1 and EcoR1 digestion and the full open reading frame confirmed by sequencing.

Other constructs used in this study are described elsewhere: GFP-CENPB (Wordeman et al., 2007), GFP-Kif15 ((Sturgill et al., 2014). GFP-Kif18A FL and Δ480 (Du et al., 2010; Stumpff et al., 2011), CMV-mCherry alone previously used to clone mCherry-MCAK (Peris et al., 2009). Scrambled control siRNA was obtained from Thermo Fisher Scientific (Silencer Negative Control #2). KBP siRNA anti-sense sequence (Kevenaar et al., 2016): 5'- UAUCAUAGUAAGCAUGUGCUU-3' (Qiagen). Kif18A siRNA anti-sense sequence (Kim et al., 2014; Stumpff et al., 2008; Stumpff et al., 2012): 5'-GCUGGAUUUCAUAAAGUGG -3' (Ambion). Kif15 siRNA anti-sense sequence (Sturgill and Ohi, 2013; Tanenbaum et al., 2009): 5'-GGACAUAAAUUGCAAAUAC-3' (Dharmacon). A SMARTpool of four siRNA sequences (Dharmacon) was used to target human Kif14.

Cell Culture and Transfections

HeLa cells were cultured at 37°C with 5% CO_2 in MEM-alpha medium (Life Technologies) containing 10% FBS plus 1% penicillin/streptomycin (Gibco). For siRNA transfections in a 24 well format, approximately 80,000 cells in 500 µL MEM-alpha medium were treated with 35 pmol siRNA and 1.5 µL RNAiMax (Life Technologies), preincubated for 20 minutes in 62.5 µL OptiMeM (Life Technologies). Cells were treated with siRNAs for 48 hours before fixing or imaging. Plasmid transfections were conducted similarly, but with 375 ng kinesin or KBP plasmid DNA (100 ng GFP-CENPB) and 2 µL LTX (Life Technologies). Plasmid transfections were incubated for 24 hours before fixing or imaging. Transfections were scaled up by well diameter as needed. For assays with sequential knockdown and plasmid transfections, the media was changed before plasmid transfection mix added.

Western Blot Analysis

For KBP western blot detection, approximately 350,000 cells were plated into a 6-well dish and transfected as described above (scaled siRNA: 150 pmol siRNA + 6 µL RNAiMax in 250 uL OptiMeM; scaled plasmid: 1.5 µg plasmid + 8 µL LTX in 250 µL OptiMeM). Cells were washed once in phosphate buffered saline (PBS: Thermo Fisher Scientific) and lysed in 200 uL PHEM Lysis Buffer (60 mM PIPES, 10mM EGTA, 4mM

$MgCl_2$, 25mM HEPES pH 6.9) with 1% Triton-X and Halt protease and phosphatase inhibitors (Thermo Fisher Scientific) by scraping the plate and incubating on ice 10 minutes. Then lysates were spun at maximum speed for 10 minutes and 180 uL supernatant added to 60 uL 4 X Laemmli Buffer prepared with βME (BioRad). Samples were run on precast 4-15% gradient gels (BioRad), transferred to low-fluorescence PVDF membrane (BioRad), blocked for 1 hour in 1:1 Odyssey blocking buffer (Li-Cor) and Tris Buffered Saline (TBS: 150 mM NaCl, and 50 mM Tris Base pH 7.4) + 0.1% TWEEN-20 (TBST). Primary antibodies against mouse-KBP (Abnova, 1:1,000) and rabbit-γ tubulin (Abcam, 1:1,000) were added in TBS overnight at 4°C. The membrane was washed with 2X TBST 5 minutes each, then secondary antibodies (goat anti-mouse IgG DyLight 800 conjugate and donkey anti-rabbit IgG DyLight 680 conjugate, both at 1:10,000, Thermo Scientific) added in 1:1 Odyssey blocking buffer and TBST for 1 hour at room temperature. The membrane was washed with 2X TBST, then 1X TBS for 5 minutes each and developed on an Odyssey CLx (Li-Cor).

Cell Fixation and Immunofluorescence

For metaphase observations, cells were treated with 20 μM MG132 (Selleck Chemicals) for 1-2 hours before fixation. No MG132 was added for anaphase observations. For spindle collapse assays, cells were collected in G2 overnight with 9 μM RO-3306 (Axxora), washed 5X with DMEM supplemented with FBS and pen/strep, then treated for 90 minutes with 5 μM MG132, followed by 90 minutes with 5 μM MG132 + 10 μM DMSO or 10 μM STLC (Sigma-Aldrich). Cells were fixed on coverslips in -20°C methanol (Fisher Scientific) plus 1% paraformaldehyde (Electron Microscopy Sciences) for 10 minutes on ice, dunked briefly and then washed 3X for 5 minutes each in TBS. Coverslips were blocked with 20% goat serum in antibody-diluting buffer (Abdil: TBS pH 7.4, 1% bovine serum albumin, 0.1% Triton-X, and 0.1% sodium azide) for 1 hr at room temperature before the primary antibodies diluted in Abdil were added for 1 hour at room temperature: mouse anti-α tubulin at 1 ug/mL (Sigma-Aldrich), mouse anti-γ-tubulin at 1 ug/mL (Sigma-Aldrich), rabbit anti-Kif18A at 2 ug/mL (Bethyl), rabbit anti-Kif15 at 1 ug/mL (Sturgill and Ohi, 2013), rabbit anti-GFP at 4 ug/mL (Molecular Probes), rabbit anti-Kif14 at 2 ug/mL (Abcam). Cells were incubated with the following primary antibodies overnight at 4°C: human anti-centromere protein (ACA) at 2.5μg/mL (Antibodies Incorporated), mouse anti-Hec1 at 0.5 ug/mL (GeneTex). All mCherry images are direct measurement of mCherry fluorescence. Incubation with 1 ug/mL goat secondary antibodies against mouse, rabbit, or human IgG conjugated to Alex Fluor 488, 594, or 647 (Molecular Probes) occurred for 1 hour at room temperature. 2X TBS 5 minute washes were performed between rounds of primary and secondary antibody incubations, finishing with 3X TBS washes before mounting with Prolong Gold anti-fade mounting medium with 4',6-Diamidine-2'-phenylindole dihydrochloride (DAPI) (Molecular Probes).

Protein Purification

His_6-Kif15-N420, His_6-Kif15-N700 and Kif18a-N480-GFP-His_6 purifications have been described previously (Reinemann et al., 2017; Stumpff et al., 2011; Sturgill et al., 2014).

GST-KBP was expressed in BL21DE3 cells with 0.4mM IPTG over night at 16ºC. Cells were pelleted and flash frozen in liquid nitrogen and stored at -80ºC. For purification,

pellets were resuspended in lysis buffer (1xPBS, 500mM NaCl, 5mM β-mercaptoethanol (β-ME), 1% NP40 and protease inhibitors (cOmplete Protease Inhibitor Cocktail tablets, Sigma-Aldrich). Lysate was incubated with 1mg/mL of lysozyme for 30 minutes on ice, followed by sonication. Lysate was clarified by centrifugation at 35,000 rpm for 1 hour at 4ºC in a Ti 45 rotor (Beckman). Clarified supernatant was incubated with 2 ml of glutathione-agarose (Sigma-Aldrich) for 1 hour at 4ºC and washed with ~200 mLs of wash buffer (1xPBS, 500mM NaCl and 5mM β-ME). Protein was eluted with 1M Tris (pH 8.0), 3M KCl and 200mM glutathione and peak fractions were buffered exchanged into storage buffer (10mM K-HEPES pH 7.7, 100mM KCl and 1mM DTT) using a PD 10 desalting column (GE Healthcare). Protein concentration was determined using Bradford assays and powdered sucrose was added 10% w/v before the protein was aliquoted, frozen in liquid nitrogen, and stored in -80ºC.

Microscopy

Cells were imaged on a Nikon Ti-E inverted microscope (Nikon Instruments) with Nikon objectives Plan Apo λ 60X 1.42NA and APO 100X 1.49 NA with a Spectra-X light engine (Lumencore) and environment chamber. The following cameras were used: Clara cooled-CCD camera (Andor) and iXon X3 EMCCD camera (Andor). The Nikon Ti-E microscope is driven by NIS Elements software (Nikon Instruments). Gliding filament assays were performed on a Nikon Elements controlled Eclipse 90i (Nikon) equipped with a 60x 1.4 NA (Nikon) objective and a Cool Snap HQ2 CCD camera (Roper). Spindle collapse assay cells were acquired using a 60X 1.4 NA objective (Olympus) on a DeltaVision Elite imaging system (GE Healthcare) equipped with a Cool SnapHQ2 charge-coupled device (CCD) camera (Roper).

Gliding Filament Assays

Flow chambers were assembled using a glass slide, a smaller No 1.5 glass coverslip and double-sided tape to create a ~20ul chamber. Approximately 1μM of Kif15-N700 or Kif18a-N480 was incubated in the chamber for 3 minutes. The chamber was then washed with 60 ul of wash buffer (WB, [1x BRB80, 1 mM MgATP, 0.5 mg/ml casein]) and next incubated with 1% Pluronic F-127 for 1 minute to passivate the surface. The chamber was again washed with 60 ul of WB and then incubated with 0.5-1 μM of Alexa-594 labelled MTs (1:10, labeled:unlabeled tubulin) for 3 minutes. The chamber was then washed with 60 ul of flow cell buffer with or without KBP (WB plus 70 mM β-ME, 0.035 mg/ml catalase, 0.2mg/ml glucose oxidase, 4.5 mg/ml glucose) and then imaged by epifluorescence microscopy. Time lapse sequences spanned 2 minutes with acquisitions captured every 2 seconds. ImageJ was used for image analysis and MT velocity was calculated by measuring the distance the MT travelled in total during the 2 minute movie (120 seconds). The average velocity of control slides from one experimental day was calculated and used to calculate the percent inhibition using the following equation,

$$\%\,Inhibition = 100 - \left(\left(\frac{Vx}{V\mu}\right) * 100\right)$$

where Vx is the velocity of a single MT and $V\mu$ is the average velocity of control MTs from that experimental day.

Co-pelleting Assays

MT-co-pelleting was performed by incubating 700nM of Kif18a-N480-GFP-His_6 or 1 μM of His_6-Kif15-N420 with 2 μM of GST-KBP in reaction buffer (10 mM K-HEPES pH 7.7, 50 mM KCl, 10 mM DTT, 1 mM $MgCl_2$ and 20 μM taxol (Sigma-Aldrich)) for 10 minutes at room temperature to promote their interaction. Kif18a-N480-GFP-His_6, His_6-Kif15-N420, and GST-KBP were clarified by spinning at 90k rpm for 10 minutes at 4ºC prior to use in assay. Next, 1 μM of taxol stabilized MTs and 1 mM AMPPNP (Sigma-Aldrich) was added to each reaction and incubated at room temperature for 15 minutes. The reaction was then spun over 150 μl of sucrose cushion (10 mM K-HEPES pH 7.7, 50 mM KCl, 20 μM taxol, 40% w/v sucrose) at 60k rpm for 20 minutes at 26ºC. 50 μl of supernatant was removed and mixed 1:1 with 2x sample buffer. The remaining supernatant was removed and the supernatant/cushion interface was washed 2x with reaction buffer. The cushion was then removed and the pellet was gently washed with reaction buffer before being resuspended in 100 μl of 1x SB. Both supernatant and pellet samples from each reaction was boiled, vortexed and 30 μl was run on a 10% SDS-PAGE gel. The gel was then stained with Coomassie for ~30 minutes and destained over night before imaging. ImageJ was used to quantify the integrated intensity of each protein band. Integrated intensity of the supernatant and pellet lanes for each reaction was combined to give yield a total protein integrated intensity value, which was used to calculate the percent of protein in the supernatant.

Live Cell Imaging

MEM-alpha media was removed from transfected cells on poly-D-lysine coated filming dishes (MatTek) and replaced with CO_2-independent imaging media (Gibco) supplemented with 10% FBS and 1% penicillin and streptomycin. Mitotic cells were identified by scanning for GFP-CENPB fluorescence at the 60X objective and imaged at the 100X objective using 0.5 um z-stacks every 5 seconds for approximately 5 minutes. After imaging, the XY position of the cell was marked and revisited within an hour of imaging to determine in the cell had divided for quality control. For mCherry or mCherry KBP expressing cells, 0.5 um z-stacks of the entire cell were taken in TRITC and GFP channels before time course imaging of GFP-CENPB.

Chromosome alignment and Kif15 localization analysis

Quantification of chromosome alignment was performed as described previously (Kim et al., 2014; Stumpff et al., 2012). Briefly, single focal planes were imaged of metaphase cells with both spindle poles in focus. The Plot Profile command in ImageJ was used to measure the distribution of ACA-labeled kinetochore fluorescence within a region of interest (ROI) defined by the length of the spindle with a set height of 17.5 um. The ACA signal intensity within the ROI was averaged along each pixel column, normalized, and plotted as a function of distance along the normalized spindle pole axis. These plots were analyzed by Gaussian fits using Igor Pro (Wavemetrics). The full width at half maximum intensity (FWHM) for the Gaussian fit and the spindle length are reported for each cell analyzed. Kif15 localization was performed similarly, but the endogenous Kif15

fluorescence was plotted across the spindle from a projection of 5, 0.2 um z-planes centered on the mid-cell plane.

Kif18A line scan analysis

Fixed and stained cells were imaged at 100X with 0.2 um z-stacks taken through the full cell. Line scans were manually measured using the α tubulin and Hec1 fluorescent intensities to identify well-defined and locally isolated kinetochore microtubules. The profile intensities for α tubulin, Hec1, and Kif18A were measured and recorded. Each channel was normalized internally to its highest value. Line scans were aligned in block by peak Hec1 intensity, and averaged for each pixel distance. Standard deviations are reported. Statistical comparisons were performed by fitting a linear regression of the accumulation slope (-0.8 μm to 0 μm) and comparing each condition to that of the control siRNA treatment using an F test.

Chromosome oscillation analysis

Live kinetochore movements were tracked and quantified as reported previously (Stumpff et al., 2008; Stumpff et al., 2012). Briefly, z-slice projections of GFP-CENPB movies were used to manually track individual kinetochore pairs with the MTrackJ plugin in ImageJ. Only kinetochore pairs near the middle of the cell were tracked; extreme peripheral kinetochore pairs were not included in the analysis. A macro was used to determine the position of the metaphase plate, which automatically fits an averaging line through thresholded GFP-CENPB signal from a time-lapse projection. Kinetochore movement parameters were quantified from kinetochore tracks in Igor Pro (Wavemetrics) and reported as the deviation from the metaphase plate (DMP) and deviation from average position (DAP). Kymographs of GFP-CENPB movements were created in ImageJ.

SUPPLEMENTAL MATERIAL

Supplemental material includes Figure S1 showing that Kif14 knockdown does not affect chromosome alignment or spindle length, Figure S2 showing an SDS-PAGE gel of purified proteins used in *in vitro* assays, and Figure S3 showing that Kif18A's C-terminal microtubule binding domain causes spindle localization in the presence of KBP overexpression Supplemental videos include example gliding filament movies for Kif15 N700 and Kif18A N480 with and without KBP (Videos S1-4) and four examples of GFP-CENPB kinetochore oscillations, one for each condition of control treatments, KBP siRNA, and mCh KBP overexpression (Videos S5-8).

ACKNOWLEDGMENTS

We thank Casper Hoogenraad's group for the generous gift of their HA-KBP plasmid. We also thank Cindy Fonseca for technical support. This work was possible through the following funding sources: NIH R01 grants to J. Stumpff (R01GM121491) and R. Ohi (R01GM086610). R. Ohi is a Scholar of the Leukemia and Lymphoma Society. H. Malaby is currently supported by a Department of Defense PRCRP Horizon Award (W81XWH-17-1-0371). The authors declare no competing financial interests.

AUTHOR CONTRIBUTIONS

H. Malaby, M. Dumas, R. Ohi, and J. Stumpff conceptualized the project and designed the experiments. H. Malaby, M. Dumas, and J. Stumpff performed the experiments. H. Malaby created the mCherry-KBP construct and performed the altered KBP expression experiments in metaphase and anaphase and kinesin overexpression in anaphase, and all Kif18A assays with the exception of the kinetochore oscillation experiments where she split the imaging with J. Stumpff. M. Dumas purified KBP and Kif15 proteins and performed the gliding filament and co-pelleting assays as well as Kif15 functional assays. H. Malaby and M. Dumas analyzed the data and assembled figures. H. Malaby wrote the manuscript. All authors reviewed and approved the final version of the manuscript.

ABBREVIATIONS

Kinesin Binding Protein (KBP)
mCherry (mCh)
Overexpression (OE)

FIGURE LEGENDS

Figure 1. KBP regulates chromosome alignment and spindle length in mitotic cells. (**A**) Western Blot against KBP, showing protein levels under KBP siRNA and mCherry-tagged (mCh) KBP transfection conditions. y-tubulin used as a loading control. (*right*) KBP knockdown quantification, obtained from quantification of three independent blots, corrected against y-tubulin and normalized to the control siRNA transfection. **, $p = 0.0047$ by unpaired t test. (**B**) mCh KBP does not bind microtubules in interphase HeLa cells. Yellow box denotes inset area. Arrows highlight occasional mCh KBP puncta that co-localize with α-tubulin. (**C**) HeLa metaphase cells knocked down with KBP siRNA or overexpressed (OE) with mCh KBP display alignment and spindle length defects. ACA, anti-centromere antibodies. (**D**) Quantification of chromosome alignment by measuring the distribution (full-width) distance at which the ACA fluorescence intensity is at half its maximum peak (FWHM). (*left*) Graphical representation of FWHM measurement. (*middle*) FWHM distance values for each cell under control siRNA, KBP siRNA, or mCh KBP OE conditions. Dotted line denotes cutoff value for hyper-aligned cells (3.3 μm), empirically determined from the control population. ‡, $p = 0.0432$ by Chi-square analysis comparing hyper-aligned populations. ****, adjusted $p < 0.0001$ with 95% confidence interval by one-way ANOVA analysis with Tukey's multiple comparisons test of full data sets. (*right*) Correlation plot of mCh KBP fluorescent intensity vs. FWHM alignment values. Dotted line is linear regression to show data trend. (**E**) (*left*) Spindle length (SL) distances for control siRNA, KBP siRNA, or mCh KBP OE cells. *, adjusted $p < 0.05$, ****, adjusted $p < 0.0001$ with 95% confidence interval by one-way ANOVA with Tukey's multiple comparisons test. (*right*) Correlation plot of mCh KBP fluorescent intensity vs. spindle lengths. Dotted line is linear regression to show data trend. Data in (D) and (E) obtained from three independent experiments with the following cell numbers: control siRNA (96), KBP siRNA (105), mCh KBP OE (34).

Figure 2. Cells deficient in Kif18A and Kif15 effect chromosome alignment and spindle length in metaphase. Metaphase cells with antibody staining for (**A**) endogenous

Kif18A or (**B**) endogenous Kif15. ACA, anti-centromere antibodies. (**C**) Quantification of FWHM (*left*) and spindle length (*right*) for each cell analyzed for each knockdown condition. Cntrl, control. n.s., not significant; ****, adjusted $p < 0.0001$ with 95% confidence interval by one-way ANOVA with Tukey's multiple comparisons test. (**D**) Quantification of Kif18A (*left*) and Kif15 (*right*) knockdown efficiencies for cells analyzed in (C). For the double knockdown quantification, one coverslip each was stained for each kinesin. ****, adjusted $p < 0.0001$ with 95% confidence interval by one-way ANOVA with Tukey's multiple comparisons test as compared to control siRNA treatment. Data in (C) and (D) obtained from two independent experiments from the following cell numbers: control siRNA (103), Kif18A siRNA (113), Kif15 siRNA (82), Kif18A and Kif15 siRNA (184).

Figure 3. KBP inhibits Kif15 and Kif18A motor function in vitro. (A) Gliding filament assay with Kif18a-N480 and KBP**.** (*left*) Representative fields showing the first frame (red) and last frame (green) of microtubule filaments in the presence or absence of KBP. Scale, 20 µm. Full movies (Videos S1 and S2) available in supplemental. (*right*) Quantification of percent inhibition of microtubule gliding for Kif18a-N480alone, or with 100 nM or 250 nM KBP present in the flow cell. (**B**) Gliding filament assay with Kif15-N700 and KBP. (*left*) Representative fields showing the first frame (red) and last frame (green) of microtubule filaments in the presence or absence of KBP. Full movies (Videos S3 and S4) available in supplemental. (*right*) Quantification of microtubule gliding velocity for Kif15-N700 alone, or with 500 nM or 250 nM KBP present in the flow cell. Data in (A) and (B) obtained from three independent experiments. ****, adjusted $p < 0.0001$ with 95% confidence interval by one-way ANOVA with Tukey's multiple comparisons test as compared to control gliding reactions. (**C**) Co-pelleting assay with Kif18A-N480, KBP, and/or microtubules (MTs). S, supernatant; P, pellet. Image is a coomassie gel. Quantification of percentage of kinesin motor present in co-pelleting fractions. Data obtained from three independent experiments. ****, adjusted $p < 0.0001$ with 95% confidence interval by one-way ANOVA with Tukey's multiple comparisons test. (**D**) Co-pelleting assay with Kif15-N420, KBP, and/or microtubules (MTs). S, supernatant. P, pellet. Image is a coomassie gel. Quantification of percentage of kinesin motor present in co-pelleting fractions. Data obtained from three independent experiments. *, adjusted $p = 0.031$ with 95% confidence interval by one-way ANOVA with Tukey's multiple comparisons test.

Figure 4. KBP overexpression alters the localization of both Kif18A and Kif15 on the mitotic spindle. (**A**) Endogenous Kif18A localization in metaphase cells upon treatment with control siRNA, KBP siRNA, or mCh KBP OE. Hec1, kinetochore marker. (**B**) Line scans measuring Kif18A accumulation on kinetochore microtubule ends. Multiple line scans combined by normalizing to peak Hec1 fluorescent signal intensity. Kif18A, green; Hec1, red; α-tubulin, blue. Solid line is average, error bars are standard deviation. (*bottom*) Overlay of average Kif18A localization for all three conditions: control siRNA, black; KBP siRNA, blue-green; mCh KBP, red. n.s, not significant; ****, $p < 0.0001$ by F test comparing slopes of linear regressions. (**C**) Endogenous Kif15 localization in metaphase cells upon treatment with control siRNA, KBP siRNA, or mCh KBP OE. (**D**) Quantification of Kif15 localization on the spindle under KBP expression conditions. The FWHM of Kif15 intensity was determined for each cell analyzed. n.s., not significant; ****, adjusted $p < 0.0001$ with 95% confidence interval by one-way ANOVA with Tukey's multiple comparisons test. Data in (B) and (D) obtained from three independent experiments each with the following cell

numbers: (B) control siRNA (21 (61 lines)), KBP siRNA (22 (63 lines)), mCh KBP OE (19 (53 lines)); (C) control siRNA (51), KBP siRNA (59), mCh KBP OE (24).

Figure 5. KBP overexpression inhibits Kif15-driven spindle stabilization. (**A**) Schematic of spindle collapse assay. (**B**) Metaphase cells expressing mCh only or mCh KBP treated with DMSO or the Eg5 inhibitor STLC, scale bar is 10 µm. (**C**) Quantification of the percentage of mitotic cells with monopolar spindles, normalized to the DMSO condition. Data obtained from three independent experiments with the following cell numbers: mCh only DMSO (103), mCh only STLC (134), mCh KBP DMSO (200), mch KBP STLC (269). **, adjusted p = 0.0058 with 95% confidence interval by two-way ANOVA with Tukey's multiple comparisons test.

Figure 6. Altered KBP expression effects kinetochore oscillatory movements. (**A**) Example traces showing the deviation from the metaphase plate (DMP) of representative kinetochore pairs for control or KBP siRNA and mCh only or mCh KBP treatments. Dotted line marks the metaphase plate. (**B**) Representative kymographs of GFP-tagged CENP-B expressing metaphase cells. Full videos available in supplemental (Videos S5-S8). (**C**) Quantification of the DMP, DAP (deviation from average position), and mCh fluorescence. DMP and DAP values are for each individual kinetochore tracked and normalized to the control siRNA or mCh only conditions. *, adjusted p < 0.05; ****, adjusted p < 0.0001 with 95% confidence interval by one-way ANOVA with Tukey's multiple comparisons test. Data obtained from the following numbers of cells over two or three independent experiments: control siRNA (10 (97 kinetochores)), KBP siRNA (12 (83 kinetochores)), mCh only (8 (69 kinetochores)), mCh KBP (7 (75 kinetochores)). For the mCherry expressing cells, a base cutoff of 1,000 background subtracted fluorescent units was required for inclusion in the data set.

Figure 7. Cells deficient in KBP or overexpressing Kif18A and/or Kif15 display multiple lagging chromosomes in anaphase. (**A**) Anaphase cells treated with control siRNA or KBP siRNA. ACA, anti-centromere antibodies. (**B**) Quantification of the percentage of lagging chromosomes under the two knockdown conditions. *, p = 0.0136 by unpaired t test. Data obtained from three independent experiments with the following cell numbers: control siRNA (66), KBP siRNA (82). (**C**) Among the cells with lagging chromosomes, quantification of the number of chromosomes lagging per cell. 1 lagging chromosome, blue; 2 lagging chromosomes, pink; more than 2 lagging chromosomes, green. White numbers are percentage for each group. Number of cells with lagging chromosomes analyzed: control siRNA (13), KBP siRNA (31). ***, p < 0.001 by Chi-square analysis. (**D**) Anaphase cells overexpressing either mCherry only, mCherry-tagged Kif18A, GFP-tagged Kif15, or both mCherry-Kif18A and GFP-tagged Kif15. Arrows point to lagging chromosomes. (**E**) Quantification of the average lagging chromosomes in a cell with increase levels of mCh only, mCh Kif18A, or GFP Kif15 overexpression. Background subtracted fluorescent intensity values are equally divided into bins (extra data points not divisible by 5 are equally divided amongst bins starting from lowest bin). Individual data points are shown in background, foreground is average number of lagging chrom0somes with standard deviations. Data obtained from seven independent data sets with the following cell numbers: mCh only (92), mCh Kif18A (28), GFP Kif15 (49). Significance: Bin 4 mCh only vs. mCh Kif18A adjusted p = 0.0044; Bin 5 mCh only vs. mCh Kif18A adjusted p < 0.0001; Bin 5 mCh only vs. GFP Kif15 adjusted p = 0.0016 with 95% confidence

interval by two-way ANOVA with Tukey's multiple comparisons test. (**F**) Breakdown of the number of lagging chromosomes or split pole phenotypes observed in the top 25% of expressing cells for each condition. no lagging chromosomes, black; 1-2 lagging chromosomes, blue; more than 2 lagging chromosomes, green; split poles, red. Data obtained from four independent data sets with the following total cell numbers: mCh only (55), mCh Kif18A (19), GFP Kif15 (23), mCh Kif18A and GFP Kif15 (18). $p < 0.0001$ by Chi-square analysis. (**G**) Average kinesin overexpression above endogenous motor. Cells were transfected with either mCh Kif18A or GFP Kif15, fixed and stained against an antibody specific to the kinesin motor in a different fluorescent channel. Anaphase cells were imaged and divided into either expressing or not expressing mCh/GFP tagged kinesins, and the background subtracted fluorescence of the antibody against each kinesin motor plotted. Average fold increase in kinesin expression above endogenous for each kinesin: mCh Kif18A (1.75), GFP Kif15 (2.16). Data obtained from two independent data sets with the following cell numbers: Kif18A not expressing mCh Kif18A (39), expressing mCh Kif18A (12), Kif15 not expressing GFP Kif15 (46), expressing GFP Kif15 (15).

Video S1. Kif15 in gliding filament assay from Figure 3. 1μM of Kif15-N700 was incubated in the chamber. Shown are Alexa-594 labelled microtubules gliding along the surface using time-lapse epifluorescence microscopy. Timestamps and scale bar included in the video.

Video S2. Kif15 with KBP in gliding filament assay from Figure 3. 1μM of Kif15-N700 was incubated in the chamber before addition of 250nM KBP. Shown are Alexa-594 labelled microtubules gliding along the surface using time-lapse epifluorescence microscopy. Timestamps and scale bar included in the video.

Video S3. Kif18A in gliding filament assay from Figure 3. 1μM of Kif18a-N480 was incubated in the chamber. Shown are Alexa-594 labelled microtubules gliding along the surface using time-lapse epifluorescence microscopy. Timestamps and scale bar included in the video.

Video S4. Kif18A with KBP in gliding filament assay from Figure 3. 1μM of Kif18a-N480 was incubated in the chamber before addition of KBP. Shown are Alexa-594 labelled microtubules gliding along the surface using time-lapse epifluorescence microscopy. Timestamps and scale bar included in the video.

Video S5. Kinetochore oscillations in control siRNA treated cells from Figure 6. HeLa cells were knocked down with control siRNAs and transfected GFP-CENPB to label kinetochores. Shown are the kinetochore oscillations in an example cell using time-lapse epifluorescence microscopy. Timestamps and scale bar included in the video.

Video S6. Kinetochore oscillations in KBP siRNA treated cells from Figure 6. HeLa cells were knocked down with KBP siRNAs and transfected GFP-CENPB to label kinetochores. Shown are the kinetochore oscillations in an example cell using time-lapse epifluorescence microscopy. Timestamps and scale bar included in the video.

Video S7. Kinetochore oscillations in mCh only expressing cells from Figure 6. HeLa cells were transfected with mCherry and GFP-CENPB to label kinetochores. Shown is the

GFP channel of kinetochore oscillations in an example cell using time-lapse epifluorescence microscopy. Timestamps and scale bar included in the video.

Video S8. Kinetochore oscillations in mCh KBP expressing cells from Figure 6. HeLa cells were transfected with mCherry-KBP and GFP-CENPB to label kinetochores. Shown is the GFP channel of kinetochore oscillations in an example cell using time-lapse epifluorescence microscopy. Timestamps and scale bar included in the video.

REFERENCES

Alves, M.M., G. Burzynski, J.M. Delalande, J. Osinga, A. van der Goot, A.M. Dolga, E. de Graaff, A.S. Brooks, M. Metzger, U.L. Eisel, I. Shepherd, B.J. Eggen, and R.M. Hofstra. 2010. KBP interacts with SCG10, linking Goldberg-Shprintzen syndrome to microtubule dynamics and neuronal differentiation. *Hum Mol Genet*. 19:3642-3651.

Bakhoum, S.F., and D.A. Compton. 2012. Kinetochores and disease: keeping microtubule dynamics in check! *Current opinion in cell biology*. 24:64-70.

Brooks, A.S., A.M. Bertoli-Avella, G.M. Burzynski, G.J. Breedveld, J. Osinga, L.G. Boven, J.A. Hurst, G.M. Mancini, M.H. Lequin, R.F. de Coo, I. Matera, E. de Graaff, C. Meijers, P.J. Willems, D. Tibboel, B.A. Oostra, and R.M. Hofstra. 2005. Homozygous nonsense mutations in KIAA1279 are associated with malformations of the central and enteric nervous systems. *Am J Hum Genet*. 77:120-126.

Brouwers, N., N. Mallol Martinez, and I. Vernos. 2017. Role of Kif15 and its novel mitotic partner KBP in K-fiber dynamics and chromosome alignment. *PloS one*. 12:e0174819.

Carleton, M., M. Mao, M. Biery, P. Warrener, S. Kim, C. Buser, C.G. Marshall, C. Fernandes, J. Annis, and P.S. Linsley. 2006. RNA interference-mediated silencing of mitotic kinesin KIF14 disrupts cell cycle progression and induces cytokinesis failure. *Molecular and cellular biology*. 26:3853-3863.

Cross, R.A., and A. McAinsh. 2014. Prime movers: the mechanochemistry of mitotic kinesins. *Nature reviews. Molecular cell biology*. 15:257-271.

Drevillon, L., A. Megarbane, B. Demeer, C. Matar, P. Benit, A. Briand-Suleau, V. Bodereau, J. Ghoumid, M. Nasser, X. Decrouy, M. Doco-Fenzy, P. Rustin, D. Gaillard, M. Goossens, and I. Giurgea. 2013. KBP-cytoskeleton interactions underlie developmental anomalies in Goldberg-Shprintzen syndrome. *Hum Mol Genet*. 22:2387-2399.

Du, Y., C.A. English, and R. Ohi. 2010. The kinesin-8 Kif18A dampens microtubule plus-end dynamics. *Current biology : CB*. 20:374-380.

Ems-McClung, S.C., Y. Zheng, and C.E. Walczak. 2004. Importin alpha/beta and Ran-GTP regulate XCTK2 microtubule binding through a bipartite nuclear localization signal. *Mol Biol Cell*. 15:46-57.

Gruneberg, U., R. Neef, X. Li, E.H. Chan, R.B. Chalamalasetty, E.A. Nigg, and F.A. Barr. 2006. KIF14 and citron kinase act together to promote efficient cytokinesis. *The Journal of cell biology*. 172:363-372.

Honnappa, S., S.M. Gouveia, A. Weisbrich, F.F. Damberger, N.S. Bhavesh, H. Jawhari, I. Grigoriev, F.J. van Rijssel, R.M. Buey, A. Lawera, I. Jelesarov, F.K. Winkler, K. Wuthrich, A. Akhmanova, and M.O. Steinmetz. 2009. An EB1-binding motif acts as a microtubule tip localization signal. *Cell*. 138:366-376.

Jiang, K., G. Toedt, S. Montenegro Gouveia, N.E. Davey, S. Hua, B. van der Vaart, I. Grigoriev, J. Larsen, L.B. Pedersen, K. Bezstarosti, M. Lince-Faria, J. Demmers, M.O. Steinmetz, T.J. Gibson, and A. Akhmanova. 2012. A Proteome-wide screen for mammalian SxIP motif-containing microtubule plus-end tracking proteins. *Current biology : CB*. 22:1800-1807.

Kevenaar, J.T., S. Bianchi, M. van Spronsen, N. Olieric, J. Lipka, C.P. Frias, M. Mikhaylova, M. Harterink, N. Keijzer, P.S. Wulf, M. Hilbert, L.C. Kapitein, E. de Graaff, A. Ahkmanova, M.O. Steinmetz, and C.C. Hoogenraad. 2016. Kinesin-

Binding Protein Controls Microtubule Dynamics and Cargo Trafficking by Regulating Kinesin Motor Activity. *Current biology : CB*. 26:849-861.
Kim, H., C. Fonseca, and J. Stumpff. 2014. A unique kinesin-8 surface loop provides specificity for chromosome alignment. *Molecular biology of the cell*. 25:3319-3329.
Kurasawa, Y., Earnshaw, W.C., Mochizuki, Y., Dohmae, N., Todokoro, K. 2004. Essential roles of Kif4 and its binding partner PRC1 in organized central spindle midzone formation. *EMBO J*. 23:3237-3248.
Ma, N., J. Titus, A. Gable, J.L. Ross, and P. Wadsworth. 2011. TPX2 regulates the localization and activity of Eg5 in the mammalian mitotic spindle. *The Journal of cell biology*. 195:87-98.
Maliga, Z., M. Junqueira, Y. Toyoda, A. Ettinger, F. Mora-Bermudez, R.W. Klemm, A. Vasilj, E. Guhr, I. Ibarlucea-Benitez, I. Poser, E. Bonifacio, W.B. Huttner, A. Shevchenko, and A.A. Hyman. 2013. A genomic toolkit to investigate kinesin and myosin motor function in cells. *Nat Cell Biol*. 15:325-334.
Mann, B.J., S.K. Balchand, and P. Wadsworth. 2017. Regulation of Kif15 localization and motility by the C-terminus of TPX2 and microtubule dynamics. *Mol Biol Cell*. 28:65-75.
Mayr, M.I., M. Storch, J. Howard, and T.U. Mayer. 2011. A non-motor microtubule binding site is essential for the high processivity and mitotic function of kinesin-8 Kif18A. *PloS one*. 6:e27471.
Nachury, M.V., T.J. Maresca, W.C. Salmon, C.M. Waterman-Storer, R. Heald, and K. Weis. 2001. Importin beta is a mitotic target of the small GTPase Ran in spindle assembly. *Cell*. 104:95-106.
Nath, S., D. Ghatak, P. Das, and S. Roychoudhury. 2015. Transcriptional control of mitosis: deregulation and cancer. *Front Endocrinol (Lausanne)*. 6:60.
Peris, L., M. Wagenbach, L. Lafanechere, J. Brocard, A.T. Moore, F. Kozielski, D. Job, L. Wordeman, and A. Andrieux. 2009. Motor-dependent microtubule disassembly driven by tubulin tyrosination. *The Journal of cell biology*. 185:1159-1166.
Prosser, S.L., and L. Pelletier. 2017. Mitotic spindle assembly in animal cells: a fine balancing act. *Nature reviews. Molecular cell biology*. 18:187-201.
Rath, O., and F. Kozielski. 2012. Kinesins and cancer. *Nature reviews. Cancer*. 12:527-539.
Reinemann, D.N., E.G. Sturgill, D.K. Das, M.S. Degen, Z. Voros, W. Hwang, R. Ohi, and M.J. Lang. 2017. Collective Force Regulation in Anti-parallel Microtubule Gliding by Dimeric Kif15 Kinesin Motors. *Current biology : CB*. 27:2810-2820 e2816.
Santamaria, A., S. Nagel, H.H.W. Sillje, and E.A. Nigg. 2008. The spindle protein CHICA mediates localization of the chromokinesin Kid to the mitotic spindle. *Current biology : CB*. 18:723-729.
Sigal, A., R. Milo, A. Cohen, N. Geva-Zatorsky, Y. Klein, Y. Liron, N. Rosenfeld, T. Danon, N. Perzov, and U. Alon. 2006. Variability and memory of protein levels in human cells. *Nature*. 444:643-646.
Stout, J.R., A.L. Yount, J.A. Powers, C. Leblanc, S.C. Ems-McClung, and C.E. Walczak. 2011. Kif18B interacts with EB1 and controls astral microtubule length during mitosis. *Mol Biol Cell*. 22:3070-3080.
Stumpff, J., Y. Du, C.A. English, Z. Maliga, M. Wagenbach, C.L. Asbury, L. Wordeman, and R. Ohi. 2011. A tethering mechanism controls the processivity and kinetochore-microtubule plus-end enrichment of the kinesin-8 Kif18A. *Molecular cell*. 43:764-775.

Stumpff, J., G. von Dassow, M. Wagenbach, C. Asbury, and L. Wordeman. 2008. The kinesin-8 motor Kif18A suppresses kinetochore movements to control mitotic chromosome alignment. *Developmental cell*. 14:252-262.

Stumpff, J., M. Wagenbach, A. Franck, C.L. Asbury, and L. Wordeman. 2012. Kif18A and chromokinesins confine centromere movements via microtubule growth suppression and spatial control of kinetochore tension. *Developmental cell*. 22:1017-1029.

Sturgill, E.G., D.K. Das, Y. Takizawa, Y. Shin, S.E. Collier, M.D. Ohi, W. Hwang, M.J. Lang, and R. Ohi. 2014. Kinesin-12 Kif15 targets kinetochore fibers through an intrinsic two-step mechanism. *Current biology : CB*. 24:2307-2313.

Sturgill, E.G., and R. Ohi. 2013. Kinesin-12 differentially affects spindle assembly depending on its microtubule substrate. *Current biology : CB*. 23:1280-1290.

Tahara, K., M. Takagi, M. Ohsugi, T. Sone, F. Nishiumi, K. Maeshima, Y. Horiuchi, N. Tokai-Nishizumi, F. Imamoto, T. Yamamoto, S. Kose, and N. Imamoto. 2008. Importin-beta and the small guanosine triphosphatase Ran mediate chromosome loading of the human chromokinesin Kid. *The Journal of cell biology*. 180:493-506.

Tanenbaum, M.E., L. Macurek, A. Janssen, E.F. Geers, M. Alvarez-Fernandez, and R.H. Medema. 2009. Kif15 cooperates with eg5 to promote bipolar spindle assembly. *Current biology : CB*. 19:1703-1711.

van Heesbeen, R.G., M.E. Tanenbaum, and R.H. Medema. 2014. Balanced activity of three mitotic motors is required for bipolar spindle assembly and chromosome segregation. *Cell Rep*. 8:948-956.

Weaver, L.N., S.C. Ems-McClung, J.R. Stout, C. LeBlanc, S.L. Shaw, M.K. Gardner, and C.E. Walczak. 2011. Kif18A uses a microtubule binding site in the tail for plus-end localization and spindle length regulation. *Current biology : CB*. 21:1500-1506.

Wordeman, L., M. Wagenbach, and T. Maney. 1999. Mutations in the ATP-binding domain affect the subcellular distribution of mitotic centromere-associated kinesin (MCAK). *Cell Biol Int*. 23:275-286.

Wordeman, L., M. Wagenbach, and G. von Dassow. 2007. MCAK facilitates chromosome movement by promoting kinetochore microtubule turnover. *The Journal of cell biology*. 179:869-879.

Wozniak, M.J., M. Melzer, C. Dorner, H.U. Haring, and R. Lammers. 2005. The novel protein KBP regulates mitochondria localization by interaction with a kinesin-like protein. *BMC Cell Biol*. 6:35.

Yount, A.L., H. Zong, and C.E. Walczak. 2015. Regulatory mechanisms that control mitotic kinesins. *Exp Cell Res*. 334:70-77.

Zhu, C., and W. Jiang. 2005. Cell cycle-dependent translocation of PRC1 on the spindle by Kif4 is essential for midzone formation and cytokinesis. *Proceedings of the National Academy of Sciences of the United States of America*. 102:343-348.

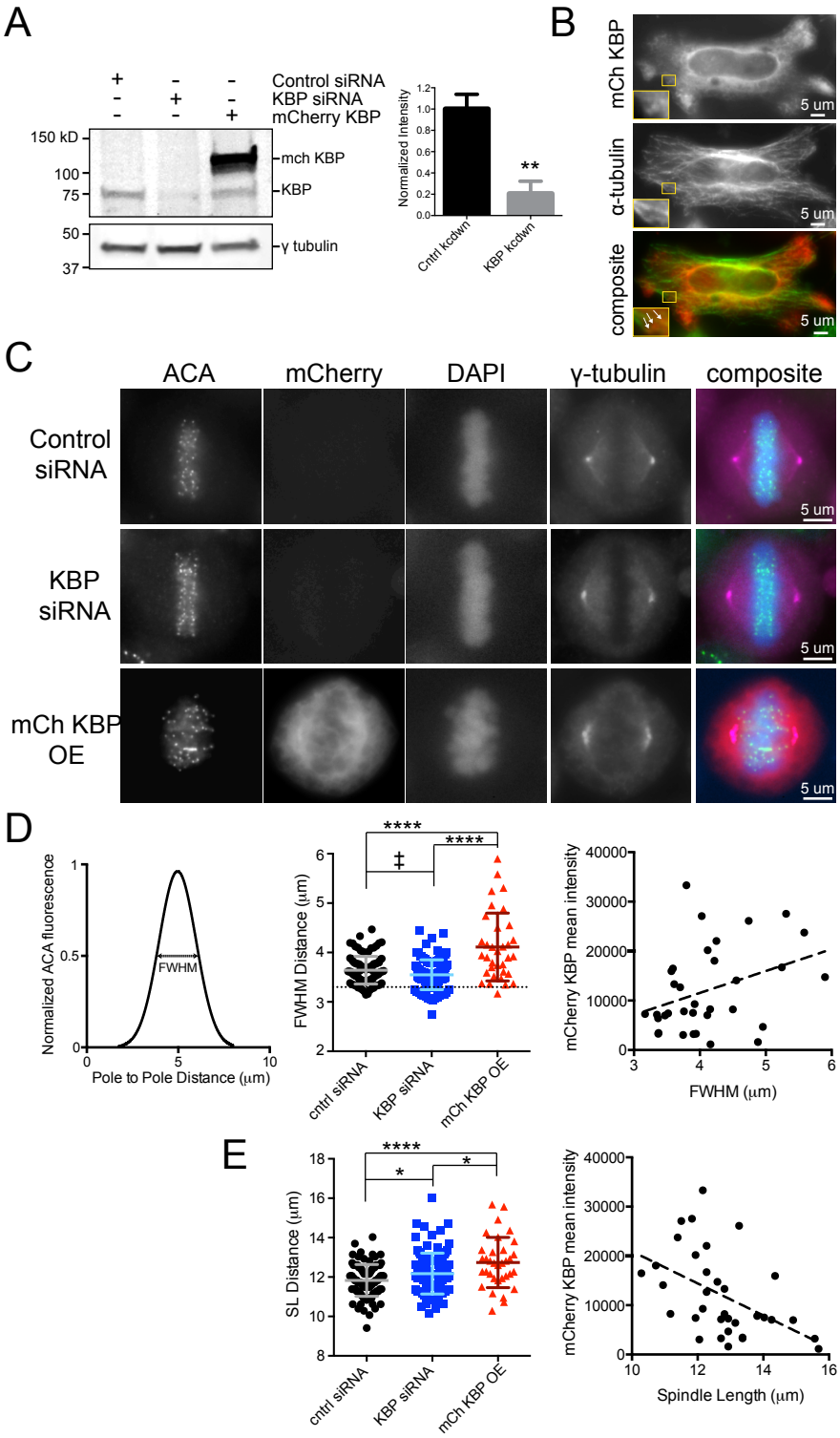
A
Control siRNA
KBP siRNA
mCherry KBP
150 kD
100
75
50
37
mch KBP
KBP
γ tubulin
Normalized Intensity
Cntrl kcdwn
KBP kcdwn
**
B
mCh KBP
α-tubulin
composite
5 um
C
ACA
mCherry
DAPI
γ-tubulin
composite
Control siRNA
KBP siRNA
mCh KBP OE
D
Normalized ACA fluorescence
FWHM
Pole to Pole Distance (μm)
FWHM Distance (μm)
cntrl siRNA
KBP siRNA
mCh KBP OE
mCherry KBP mean intensity
FWHM (μm)
E
SL Distance (μm)
Spindle Length (μm)

Figure 1

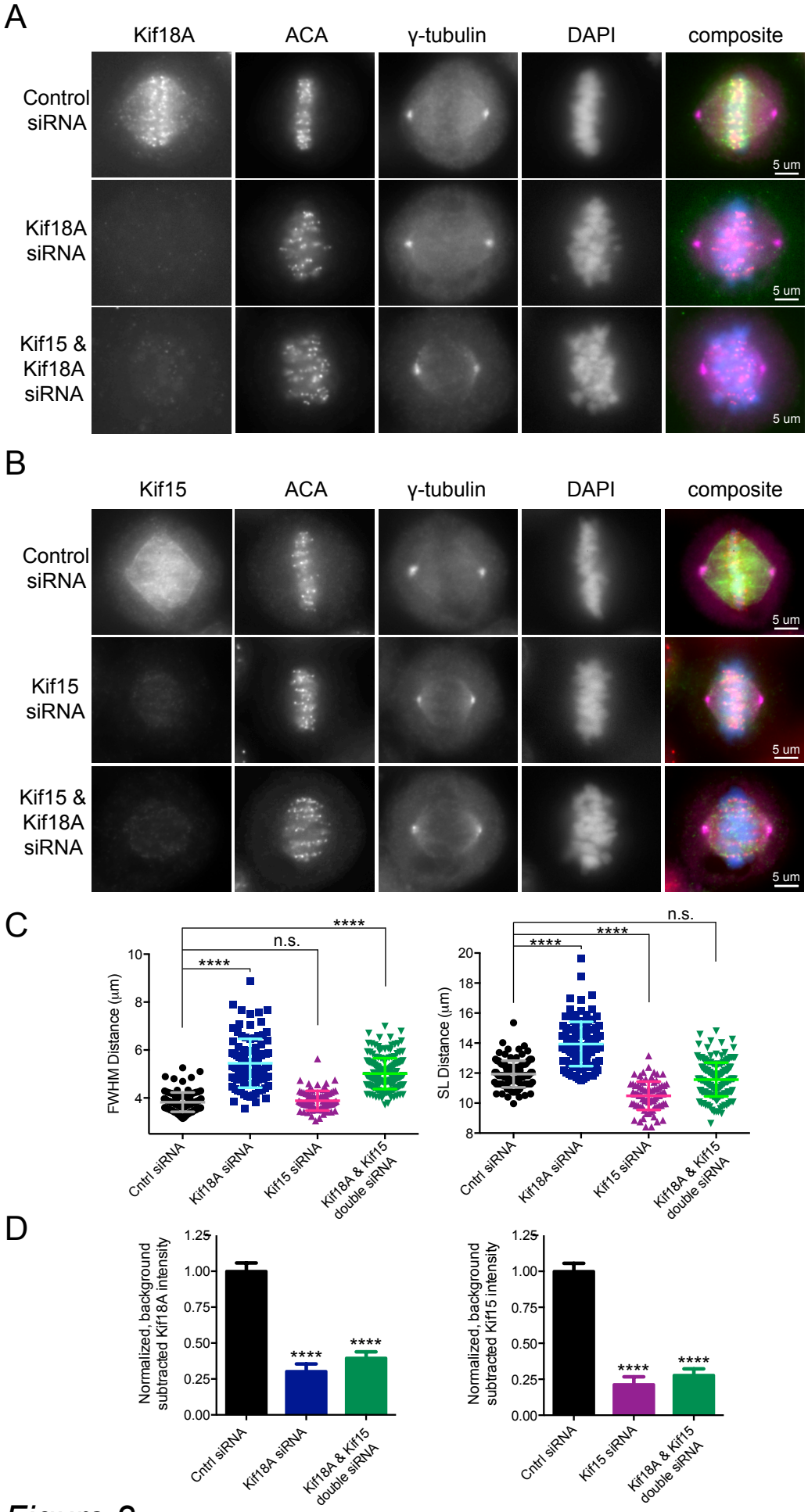
A
Kif18A
ACA
γ-tubulin
DAPI
composite
Control siRNA
Kif18A siRNA
Kif15 & Kif18A siRNA
5 um
B
Kif15
ACA
γ-tubulin
DAPI
composite
Control siRNA
Kif15 siRNA
Kif15 & Kif18A siRNA
5 um
C
FWHM Distance (µm)
SL Distance (µm)
****
n.s.
Cntrl siRNA
Kif18A siRNA
Kif15 siRNA
Kif18A & Kif15 double siRNA
D
Normalized, background subtracted Kif18A intensity
Normalized, background subtracted Kif15 intensity
****
Cntrl siRNA
Kif18A siRNA
Kif15 siRNA
Kif18A & Kif15 double siRNA

Figure 2

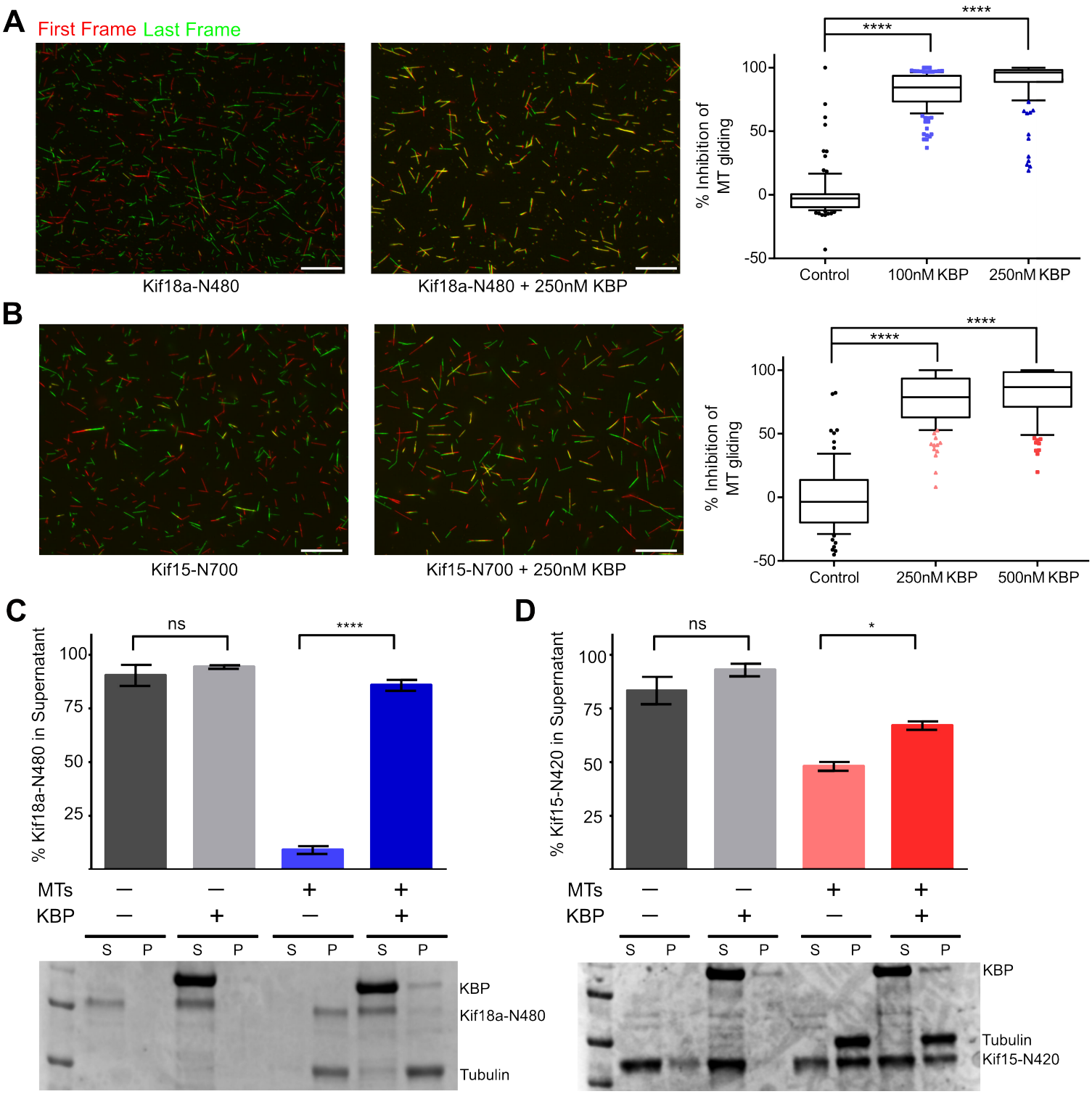
A
First Frame Last Frame
Kif18a-N480
Kif18a-N480 + 250nM KBP
% Inhibition of MT gliding
100
50
0
-50
****
****
Control
100nM KBP
250nM KBP
B
Kif15-N700
Kif15-N700 + 250nM KBP
% Inhibition of MT gliding
100
50
0
-50
****
****
Control
250nM KBP
500nM KBP
C
% Kif18a-N480 in Supernatant
100
75
50
25
ns
****
MTs – – + +
KBP – + – +
S P S P S P S P
KBP
Kif18a-N480
Tubulin
D
% Kif15-N420 in Supernatant
100
75
50
25
ns
*
MTs – – + +
KBP – + – +
S P S P S P S P
KBP
Tubulin
Kif15-N420

Figure 3

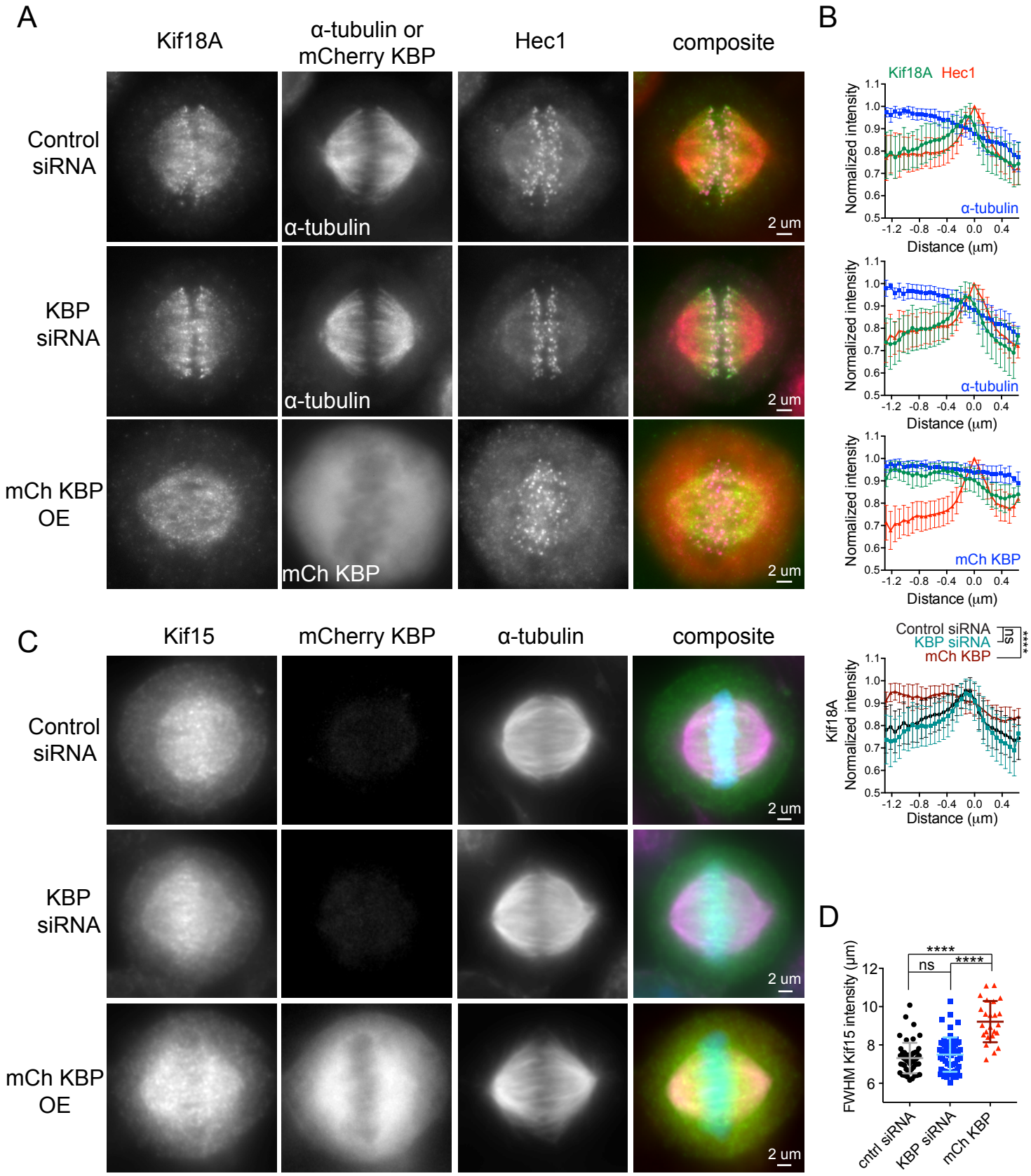
A
Kif18A
α-tubulin or mCherry KBP
Hec1
composite
Control siRNA
KBP siRNA
mCh KBP OE
α-tubulin
mCh KBP
2 um
B
Kif18A Hec1
Normalized intensity
Distance (μm)
α-tubulin
mCh KBP
C
Kif15
mCherry KBP
α-tubulin
composite
Control siRNA
KBP siRNA
mCh KBP OE
Control siRNA
KBP siRNA
mCh KBP
ns
****
Kif18A Normalized intensity
D
FWHM Kif15 intensity (μm)
****
ns
****
cntrl siRNA
KBP siRNA
mCh KBP

Figure 4

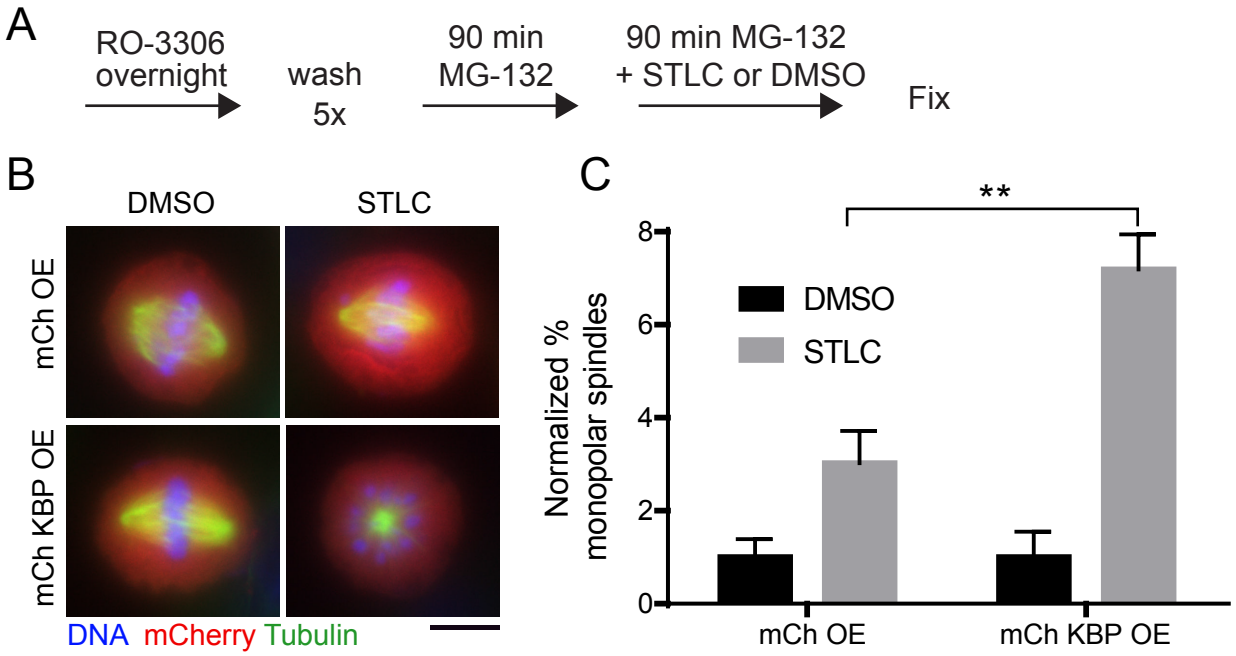
A
RO-3306
overnight
wash
5x
90 min
MG-132
90 min MG-132
+ STLC or DMSO
Fix
B
DMSO
STLC
mCh OE
mCh KBP OE
DNA mCherry Tubulin
C
**
DMSO
STLC
Normalized %
monopolar spindles
0
2
4
6
8
mCh OE
mCh KBP OE

Figure 5

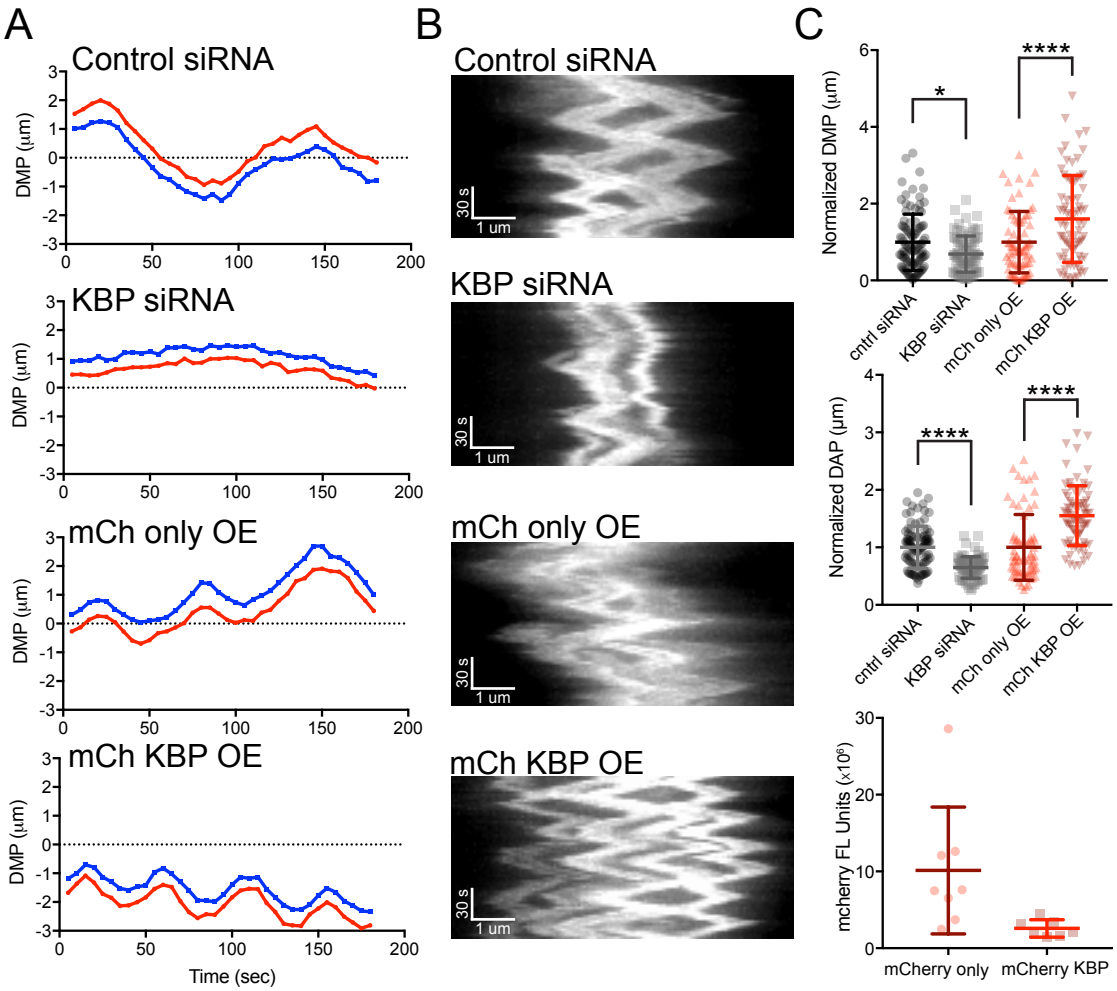
A
Control siRNA
KBP siRNA
mCh only OE
mCh KBP OE
DMP (µm)
Time (sec)
B
Control siRNA
KBP siRNA
mCh only OE
mCh KBP OE
30 s
1 um
C
Normalized DMP (µm)
Normalized DAP (µm)
cntrl siRNA
KBP siRNA
mCh only OE
mCh KBP OE
mcherry FL Units (x10⁶)
mCherry only
mCherry KBP

Figure 6

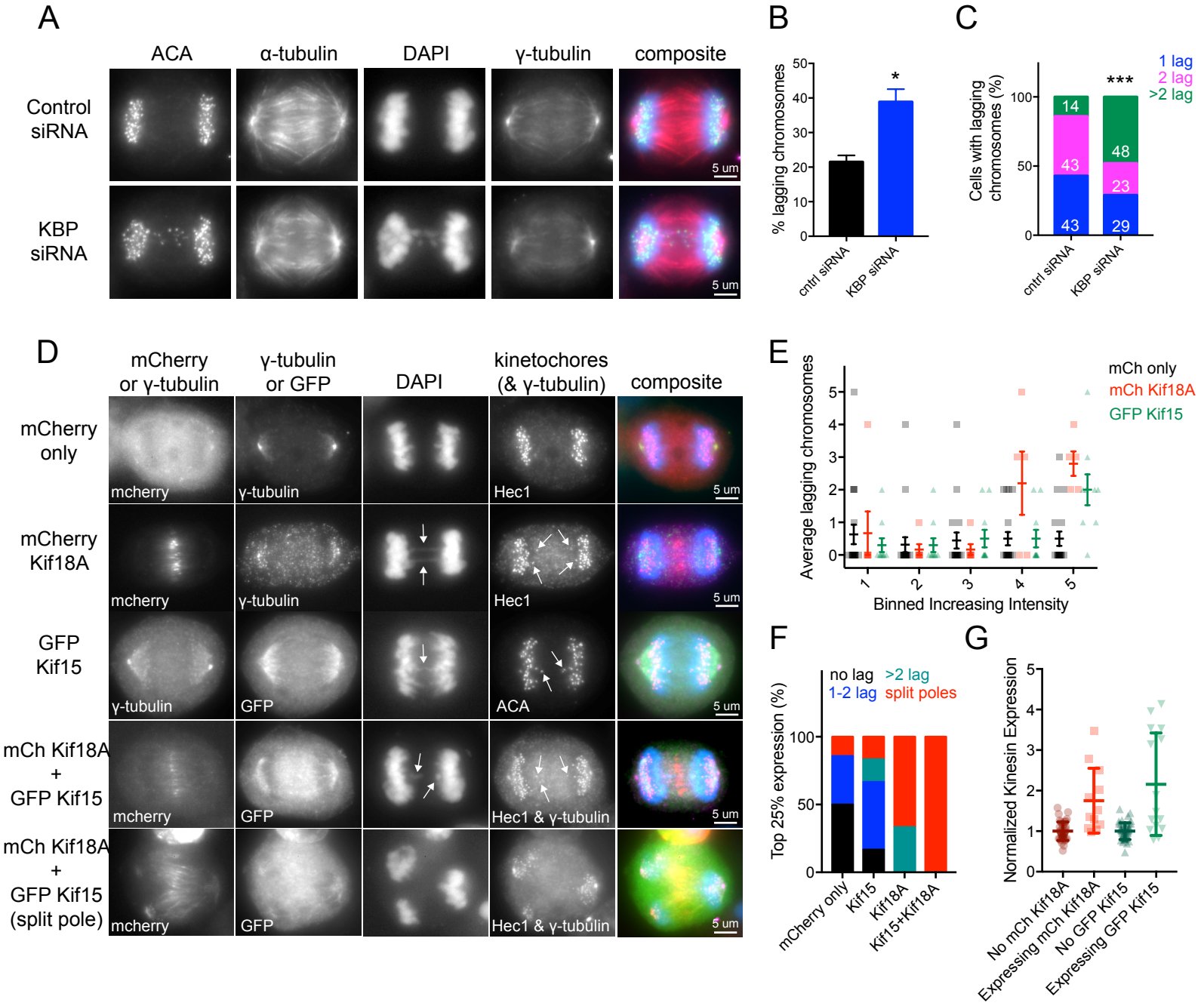
A
ACA
α-tubulin
DAPI
γ-tubulin
composite
Control siRNA
KBP siRNA
5 um
B
% lagging chromosomes
cntrl siRNA
KBP siRNA
C
Cells with lagging chromosomes (%)
1 lag
2 lag
>2 lag
14
43
43
48
23
29
D
mCherry or γ-tubulin
γ-tubulin or GFP
DAPI
kinetochores (& γ-tubulin)
composite
mCherry only
mCherry Kif18A
GFP Kif15
mCh Kif18A + GFP Kif15
mCh Kif18A + GFP Kif15 (split pole)
mcherry
γ-tubulin
Hec1
GFP
ACA
Hec1 & γ-tubulin
E
Average lagging chromosomes
Binned Increasing Intensity
mCh only
mCh Kif18A
GFP Kif15
F
Top 25% expression (%)
no lag
>2 lag
1-2 lag
split poles
mCherry only
Kif15
Kif18A
Kif15+Kif18A
G
Normalized Kinesin Expression
No mCh Kif18A
Expressing mCh Kif18A
No GFP Kif15
Expressing GFP Kif15

Figure 7